Rensselaer Polytechnic Institute
Department of Mathematical Sciences
Troy, New York 12180

Annual Report for

"Development of Numerical Methods for Various Mathematical Models of High Speed Reactive and Nonreactive Flow"

Submitted by:
Donald W. Schwendeman
Professor of Mathematical Sciences

ANNUAL REPORT
For the period ending January 31, 2008.

Prepared for:
University of California
Lawrence Livermore National Laboratory
Attn: Jill Dunaway
P.O. Box 808, L-561
Livermore, CA 94551

Under:
LLNL subcontract number B548468
RPI contract number A30498

DISCLAIMER
This document was prepared as an account of work sponsored by an agency of the United States Government. Neither the United States Government nor the University of California nor any of their employees, makes any warranty, express or implied, or assumes any legal liability or responsibility for the accuracy, completeness, or usefulness of any information, apparatus, product, or process disclosed, or represents that its use would not infringe privately owned rights. Reference herein to any specific commercial product, process, or service by trade name, trademark, manufacturer, or otherwise, does not necessarily constitute or imply its endorsement, recommendation, or favoring by the United States Government or the University of California. The views and opinions of authors expressed herein do not necessarily state or reflect those of the United States Government or the University of California, and shall not be used for advertising or product endorsement purposes. Work performed under the auspices of the U.S. Department of Energy by Lawrence Livermore National Laboratory under Contract W-7405-ENG-48.

Annual Report on

LLNL Subcontract B548468

Development of Numerical Methods for Various Mathematical Models of High Speed Reactive and Nonreactive Flow

Donald W. Schwendeman

1 Project Overview

The work carried out under this subcontract involved the development and use of adaptive, parallel numerical methods for the accurate solution of various mathematical models of high-speed reactive and nonreactive flows. The current focus is on a model for heterogeneous solid explosives and on the development of a parallel framework in which to carry out the numerical calculations of the model equations (and other sets of partial differential equations). In particular, work has continued on a two-phase, Baer-Nunziato-type model of reactive flow. At a basic level, the model involves a system of nonlinear hyperbolic partial differential equations, and numerical methods have been developed to solve the system of equations accurately. The numerical method is a high-resolution, shock-capturing scheme of Godunov type and employes a Runge-Kutta type error-control scheme to compute the stiff source terms in the equations. Adaptive mesh refinement (AMR) is used to resolve fine-scale features of the two-phase flow, such as a the structure of a detonation wave (including layers of rapid relaxation between phases), and composite overlapping grids are used to handle complex flow geometries in either two or three dimensions. An extension of the code to run in parallel for the reactive and non-reactive Euler equations (and other equations including those for two-phase reactive flow) has been developed. The code is part of the *Overture-CG* software, a collection of codes designed to handle multi-physics applications (including the *OverBlown* set of flow solvers [1, 2]). The development has occurred in close collaboration with Bill Henshaw and Lori Diachin, and other members of the Overture group within CASC.

During the period of this subcontract, a number of tasks were accomplished, including

- the further development of a numerical method for a model of two-phase reactive flow in two space dimensions,
- the further development of a parallel method for reactive and non-reactive compressible flow in three dimensions, and
- the completion of a paper on parallel computation of three-dimensional flows using overlapping grids with adaptive mesh refinement.

These items are discussed in more detail in Section 3 below.

2 Dissemination of Results

Results of the subcontract work were central to the following presentations:

1. "An Augmented Ignition-and-Growth Model that Accounts for Desensitization," Invited lecture at the LANL HE Review Meeting, Los Alamos National Laboratory, October 4, 2006.

2. "A High-Resolution Godunov Method for Reactive and Nonreactive Multi-Material Flow on Overlapping Grids," Invited minisymposium talk at the SIAM Conference on Computational Science and Engineering, Costa Mesa, CA, February 22, 2007.

3. "Detonation Evolution and Structure for a Model of Two-Phase Reactive Flow," Invited minisymposium talk at ICIAM 07, Zurich, Switzerland, July 19, 2007.

4. "Mathematical Models of Detonation in Single and Multi-Phase Reactive Flow," Invited talk at the AMS Western Section Meeting, Albuquerque, NM, October 13, 2007.

Results of this subcontract and previous ones were central to the following papers:

1. A.K. Kapila, D.W. Schwendeman, J.B. Bdzil and W.D. Henshaw, *A study of detonation diffraction in the ignition-and-growth model*, Combust. Theory and Modeling, 11 (2007), pp. 781–822.

2. J.W. Banks, D.W. Schwendeman, A.K. Kapila and W.D. Henshaw, *A high-resolution Godunov method for compressible multi-fluid flows on overlapping grids*, J. Comput. Phys., 223 (2007), pp. 262–297.

3. J.W. Banks, D.W. Schwendeman, A.K. Kapila and W.D. Henshaw, *A study of detonation propagation and diffraction with compliant confinement*, Combust. Theory Modeling, submitted.

4. W.D. Henshaw and D.W. Schwendeman, *Parallel computation of three-dimensional flows using overlapping grids with adaptive mesh refinement*, J. Comput. Phys., submitted.

3 Project Highlights

3.1 A model of two-phase reactive flow

A numerical method for a model of two-phase reactive flow has been developed. The approach generates well-resolved and accurate solutions economically, and treats rationally the nozzling terms that render the otherwise hyperbolic model incapable of a conservative representation. The method has been used during past years of the subcontract to investigate a broad range of the parameter space for a particular choice of the reaction-rate model and for a one-dimensional piston-driven flow. The focus during this past year was to investigate the behavior of solutions for two-dimensional flows. This study led to a re-examination of the model and an investigation of more complex reaction-rate models as is discussed below.

3.1.1 Governing equations

In two dimensions, the governing equations of the two-phase model have the form

$$\frac{\partial}{\partial t}\mathbf{u} + \frac{\partial}{\partial x_x}\mathbf{f}_1(\mathbf{u}) + \frac{\partial}{\partial x_2}\mathbf{f}_2(\mathbf{u}) = \mathbf{h}_1(\mathbf{u})\frac{\partial \bar{\alpha}}{\partial x_1} + \mathbf{h}_2(\mathbf{u})\frac{\partial \bar{\alpha}}{\partial x_2} + \mathbf{k}(\mathbf{u}), \tag{1}$$

where

$$\mathbf{u} = \begin{bmatrix} \bar{\alpha} \\ \bar{\alpha}\bar{\rho} \\ \bar{\alpha}\bar{\rho}\bar{u}_1 \\ \bar{\alpha}\bar{\rho}\bar{u}_2 \\ \bar{\alpha}\bar{\rho}\bar{E} \\ \alpha\rho \\ \alpha\rho u_1 \\ \alpha\rho u_2 \\ \alpha\rho E \end{bmatrix}, \qquad \mathbf{f}_1(\mathbf{u}) = \begin{bmatrix} 0 \\ \bar{\alpha}\bar{\rho}\bar{u}_1 \\ \bar{\alpha}(\bar{\rho}\bar{u}_1^2 + \bar{p}) \\ \bar{\alpha}\bar{\rho}\bar{u}_1\bar{u}_2 \\ \bar{\alpha}\bar{u}_1(\bar{\rho}\bar{E} + \bar{p}) \\ \alpha\rho u_1 \\ \alpha(\rho u_1^2 + p) \\ \alpha\rho u_1 u_2 \\ \alpha u_1(\rho E + p) \end{bmatrix}, \qquad \mathbf{f}_2(\mathbf{u}) = \begin{bmatrix} 0 \\ \bar{\alpha}\bar{\rho}\bar{u}_2 \\ \bar{\alpha}\bar{\rho}\bar{u}_1\bar{u}_2 \\ \bar{\alpha}(\bar{\rho}\bar{u}_2^2 + \bar{p}) \\ \bar{\alpha}\bar{u}_2(\bar{\rho}\bar{E} + \bar{p}) \\ \alpha\rho u_2 \\ \alpha\rho u_1 u_2 \\ \alpha(\rho u_2^2 + p) \\ \alpha u_2(\rho E + p) \end{bmatrix},$$

$$\mathbf{h}_1(\mathbf{u}) = \begin{bmatrix} -\bar{u}_1 \\ 0 \\ +p \\ 0 \\ +p\bar{u}_1 \\ 0 \\ -p \\ 0 \\ -p\bar{u}_1 \end{bmatrix}, \qquad \mathbf{h}_2(\mathbf{u}) = \begin{bmatrix} -\bar{u}_2 \\ 0 \\ 0 \\ +p \\ +p\bar{u}_2 \\ 0 \\ 0 \\ -p \\ -p\bar{u}_2 \end{bmatrix}, \qquad \mathbf{k}(\mathbf{u}) = \begin{bmatrix} \mathcal{F} + \mathcal{C}/\bar{\rho} \\ +\mathcal{C} \\ +\mathcal{M}_1 \\ +\mathcal{M}_2 \\ +\mathcal{E} - p\mathcal{F} \\ -\mathcal{C} \\ -\mathcal{M}_1 \\ -\mathcal{M}_2 \\ -\mathcal{E} + p\mathcal{F} \end{bmatrix}.$$

Here, α, ρ, (u_1, u_2) and p denote the volume fraction, density, velocity and pressure of the gas phase, respectively, and $\bar{\alpha}$, $\bar{\rho}$, $(\bar{u}_1, \bar{u}_2)$ and $\bar{p}$ denote the analogous quantities of the solid phase. (The bar superscript is used throughout to indicate solid phase quantities.) The total energies are given by

$$E = \frac{p}{(1-\gamma)\rho(1+b\rho)} + \frac{1}{2}\left(u_1^2 + u_2^2\right), \qquad \bar{E} = \frac{\bar{p} + \bar{\gamma}\bar{\pi}}{(\bar{\gamma}-1)\bar{\rho}} + \frac{1}{2}\left(\bar{u}_1^2 + \bar{u}_2^2\right) + B(\bar{\alpha}) + q,$$

where γ and $\bar{\gamma}$ are ratios of specific heats, b is a virial gas coefficient, $\bar{\pi}$ is a solid stiffening pressure, q is a heat release, and $B(\bar{\alpha})$ is the so-called compaction potential (see [3]). Following [4], we take

$$B(\bar{\alpha}) = \frac{(p_0 - \bar{p}_0)(2-\bar{\alpha}_0)^2}{\bar{\alpha}_0\bar{\rho}_0 \ln(1-\bar{\alpha}_0)} \ln\left[\left(\frac{2-\bar{\alpha}_0}{2-\bar{\alpha}}\right)\frac{(1-\bar{\alpha})^{(1-\bar{\alpha})/(2-\bar{\alpha})}}{(1-\bar{\alpha}_0)^{(1-\bar{\alpha}_0)/(2-\bar{\alpha}_0)}}\right],$$

where p_0, $\bar{p}_0$, $\bar{\alpha}_0$ and $\bar{\rho}_0$ are given by a reference ambient state. Finally, the volume fractions satisfy the saturation constraint,

$$\alpha + \bar{\alpha} = 1,$$

which closes the system of equations.

The first equation in (1) describes the compaction dynamics of the two-phase flow, while the remaining equations represent the balance of mass, momentum and energy for each phase. The nozzling terms are the first two terms on the right hand side of (1) and $\mathbf{k}(\mathbf{u})$ gives the exchange of mass, momentum and energy between phases due to compaction, drag, heat transfer, and chemical reaction (see [5, 3]). The rate of compaction is given by

$$\mathcal{F} = -\frac{\alpha\bar{\alpha}}{\mu_c}(p - \bar{p} + \beta),$$

where μ_c is the compaction viscosity and $\beta = \bar{\alpha}\bar{\rho}B'(\bar{\alpha})$ is the configuration pressure. The exchange of mass due to chemical reaction is given by $\mathcal{C}$. The form for $\mathcal{C}$ depends on the assumed reaction kinetics, and two forms have been considered as discussed below. The exchange of momentum is given by

$$\mathcal{M}_i = \frac{u_i + \bar{u}_i}{2}\mathcal{C} + \delta(u_i - \bar{u}_i), \qquad i = 1 \text{ or } 2,$$

where δ is a drag coefficient. Finally, the exchange of energy is given by

$$\mathcal{E} = \left(\bar{E} + \frac{\beta}{\bar{\rho}}\right)\mathcal{C} + \left(\delta + \frac{\mathcal{C}}{2}\right)\left[\bar{u}_1(u_1 - \bar{u}_1) + \bar{u}_2(u_2 - \bar{u}_2)\right] + \mathcal{H}(T - \bar{T}),$$

where $\mathcal{H}$ is a heat transfer coefficient, and T and $\bar{T}$ are temperatures of the gas and solid phases, respectively. These temperatures are given by

$$C_v T = \frac{p}{(\gamma - 1)\rho(1 + b\rho)}, \qquad \bar{C}_v \bar{T} = \frac{\bar{p} + \bar{\gamma}\bar{\pi}}{(\bar{\gamma} - 1)\bar{\rho}},$$

where C_v and $\bar{C}_v$ are specific heats at constant volume.

3.1.2 Reaction rate models

Two reaction rate models have been considered. The first is a relatively simple one-stage, ignition-pressure model which takes the form

$$\mathcal{C} = \begin{cases} 0 & \text{if } p < p_{\text{ig}}, \\ -\sigma\bar{\alpha}\bar{\rho}(p - p_{\text{ig}}) & \text{if } p \geq p_{\text{ig}}, \end{cases}$$

where σ is a rate constant and p_{ig} is an ignition pressure. This model was used in [6] to study detonation evolution and structure in one space dimension. For this study, evolution to detonation occurred as a result of a relatively low-speed piston impact. In the early stages of the evolution, a compaction wave develops and the gas pressure rises accordingly. This initial pressure rise, however, is relatively small (as compared to the values of the gas pressure in a steady detonation) and thus a correspondingly small value for the ignition pressure, p_{ig}, is required to initiate a reaction for this model. As a result of this small value for p_{ig}, it was found in later two-dimensional corner-turning studies that the detonation showed a negligible weakening in its post-diffracted state which does not agree with experimental evidence.

A more complex two-stage reaction rate was developed in part to better model detonation diffraction behavior. It incorporates an "ignition" stage which is following by a "burn" stage. As the explosive is compressed, it is assumed that the density of hot-spot cites increases with the volume fraction of the solid and with the work supplied to the material by compaction. If the volume fraction of the solid and the work by compaction exceeds an assumed threshold, then the ignition reaction is turned on. This reaction, once on, is assumed to remain active provided the volume fraction of the solid stays above its ambient value. If the ignition reaction is vigorous enough, i.e. if there is a sufficient density of hot spots, then a "burn" reaction is assumed to commence which results in the release of the bulk of the chemical energy via the consumption of the solid grains.

For the two-stage model, an addition "reaction progress" variable is needed. This variable, call it ϕ say, is governed by the equation

$$\frac{\partial \phi}{\partial t} + \bar{u}_1 \frac{\partial \phi}{\partial x_1} + \bar{u}_2 \frac{\partial \phi}{\partial x_2} = \mathcal{K}_{\text{ign}} + \mathcal{K}_{\text{burn}},$$

where $(\bar{u}_1, \bar{u}_2)$ is the velocity of the solid phase, and $\mathcal{K}_{\text{ign}}$ and $\mathcal{K}_{\text{burn}}$ are the rates for the ignition and burn reactions, respectively. For $\bar{\alpha} > \bar{\alpha}_0$, where $\bar{\alpha}_0$ is the ambient value of the volume fraction of the solid, the rate for the ignition reaction is taken to be

$$\mathcal{K}_{\text{ign}} = \begin{cases} \sigma_{\text{ign}} \left[\dfrac{(\bar{\alpha} - \bar{\alpha}_0)(1 - \bar{\alpha})^2}{(1 - \bar{\alpha}_0)^3} \right] & \text{if } \mathcal{T}(\bar{\alpha}, p\mathcal{F}) > 0 \text{ or } \phi > \phi_\epsilon, \\ 0 & \text{otherwise.} \end{cases}$$

Here, σ_{ign} is the strength of the ignition rate, ϕ_ϵ is a small parameter and $\mathcal{T}(\bar{\alpha}, p\mathcal{F}) = 0$ defines the ignition threshold boundary. At present, we use

$$\mathcal{T}(\bar{\alpha}, p\mathcal{F}) = \frac{p\mathcal{F}}{(p\mathcal{F})_{\text{ref}}} - \left(\frac{1}{\bar{\alpha} - \bar{\alpha}_0} - \frac{1}{1 - \bar{\alpha}_0} \right),$$

where $(p\mathcal{F})_{\text{ref}}$ is a reference scale for the work supplied by compaction. The idea is that initially when $\phi = 0$, the ignition rate is off until $\mathcal{T}(\bar{\alpha}, p\mathcal{F}) > 0$ first occurs. Once the rate turns on and ϕ becomes greater than ϕ_ϵ, then the rate remains on until $\bar{\alpha}$ drops below $\bar{\alpha}_0$. It is assumed that once the volume fraction of the solid becomes too low (below $\bar{\alpha}_0$ say), the solid grains are too far apart to support ignition due to the formation of hot spots. The rate for the burn reaction is assumed to have the form

$$\mathcal{K}_{\text{burn}} = \begin{cases} \sigma_{\text{burn}} \left(p - p_{\text{min}} \right) & \text{if } p > p_{\text{min}} \text{ and } \phi > \phi_{\text{min}}, \\ 0 & \text{otherwise,} \end{cases}$$

where σ_{burn} is the strength of the burn rate, and p_{min} and ϕ_{min} are switches for the burn reaction. Finally, the two rates are combined to give

$$\mathcal{C} = -\bar{\alpha}\bar{\rho} \left(\mathcal{K}_{\text{ign}} + \mathcal{K}_{\text{burn}} \right),$$

which appears in the various components of the source term $\mathbf{k}(\mathbf{u})$ in (1).

3.1.3 Numerical method and sample results

The numerical approach for the governing equations in (1) with either of the two reaction rates discussed in section 3.1.2 follows that described in [6, 7] for the two-phase model in one space dimension. The extension to two-dimensional flow on overlapping grids uses the approach discussed in [8, 9] for the reactive Euler equations. The discretization takes place on an overlapping grid which covers the physical domain of interest. The overlapping grid consists of a collection of curvilinear grids each defined by a mapping from the unit square in computational space to a portion of the domain in physical space. A discretization of the governing equations is applied to each component grid in computational space. The

discretization is a second-order Strang-type fractional step method consisting of a "hydro step" for the equations

$$\frac{\partial}{\partial t}\mathbf{u} + \frac{\partial}{\partial x_x}\mathbf{f}_1(\mathbf{u}) + \frac{\partial}{\partial x_2}\mathbf{f}_2(\mathbf{u}) = \mathbf{h}_1(\mathbf{u})\frac{\partial \bar{\alpha}}{\partial x_1} + \mathbf{h}_2(\mathbf{u})\frac{\partial \bar{\alpha}}{\partial x_2},$$

and a "source step" for the equations

$$\frac{\partial}{\partial t}\mathbf{u} = \mathbf{k}(\mathbf{u}).$$

The discretization for the hydro step is a second-order Godunov-type method, and it follows the approach discussed in detail in [7]. The numerical method for the ordinary differential equations in the source step uses a second-order Runge-Kutta error-control method. Adaptive mesh refinement is also used in the time-stepping procedure to locally increase the grid resolution. This is particularly apt for the two-phase model whose solutions of interest posses thin layers of rapid relaxation between the phases as well as rapid chemical reaction, and posses shocks and contacts in both of the phases.

The images shown Figure 1 illustrate the type of two-phase reactive flow problem under consideration. In this problem, a steady *compaction-led* detonation (see [6] for a detailed discussion of two-phase detonation structures) travels down a rigidly confined two-dimensional rate stick. At $t = 1$, the detonation reaches a rate stick of a larger width where it turns a 90° corner into the larger rate stick. The detonation weakens as it diffracts around the corner, and it is of interest to determine the time-dependent behavior of the detonation in the post-diffracted state. In particular, it is of interest to determine whether regions of only partially reacted material, so-called dead zones, remain behind the weakened detonation. Experimental results indicate that dead zones exist (see [10] for example), and these zones have been studied using other reactive flow models (see [11] for example). For the present two-phase flow model, the results shown in the figure employ the two-stage rate discussed in section 3.1.2. The ambient state of the explosive (with subscript 0), equation-of-state parameters, and parameters chosen for the relaxation terms and reaction rate are given in Table 1. Layers of compaction are shown in pink in the images of the volume fraction of the solid (shown on the left). In the post-diffracted state, the compaction layer thins as a result of a decoupling of the burn reaction behind it. Behind the weakened compaction layer, a dead zone appears near the vertical wall of the larger rate stick. In this region, the gas pressure (shown in the images on the right) is too low to support the burn reaction. The results shown here are preliminary and more work is needed to study the solutions in detail and to refine the model.

3.2 Parallel computation of three-dimensional flow

A numerical approach has been developed for the parallel computation of three-dimensional flow (and other problems) on overlapping grids with adaptive mesh refinement (AMR). The numerical approach is implemented on parallel distributed-memory computers using a domain-decomposition approach. The implementation is flexible so that each base grid within the overlapping grid structure and its associated refinement grids can be independently partitioned over a chosen set of processors. The partitioning is specified to balance the computational work across the processors, and this is done using a modified bin-packing

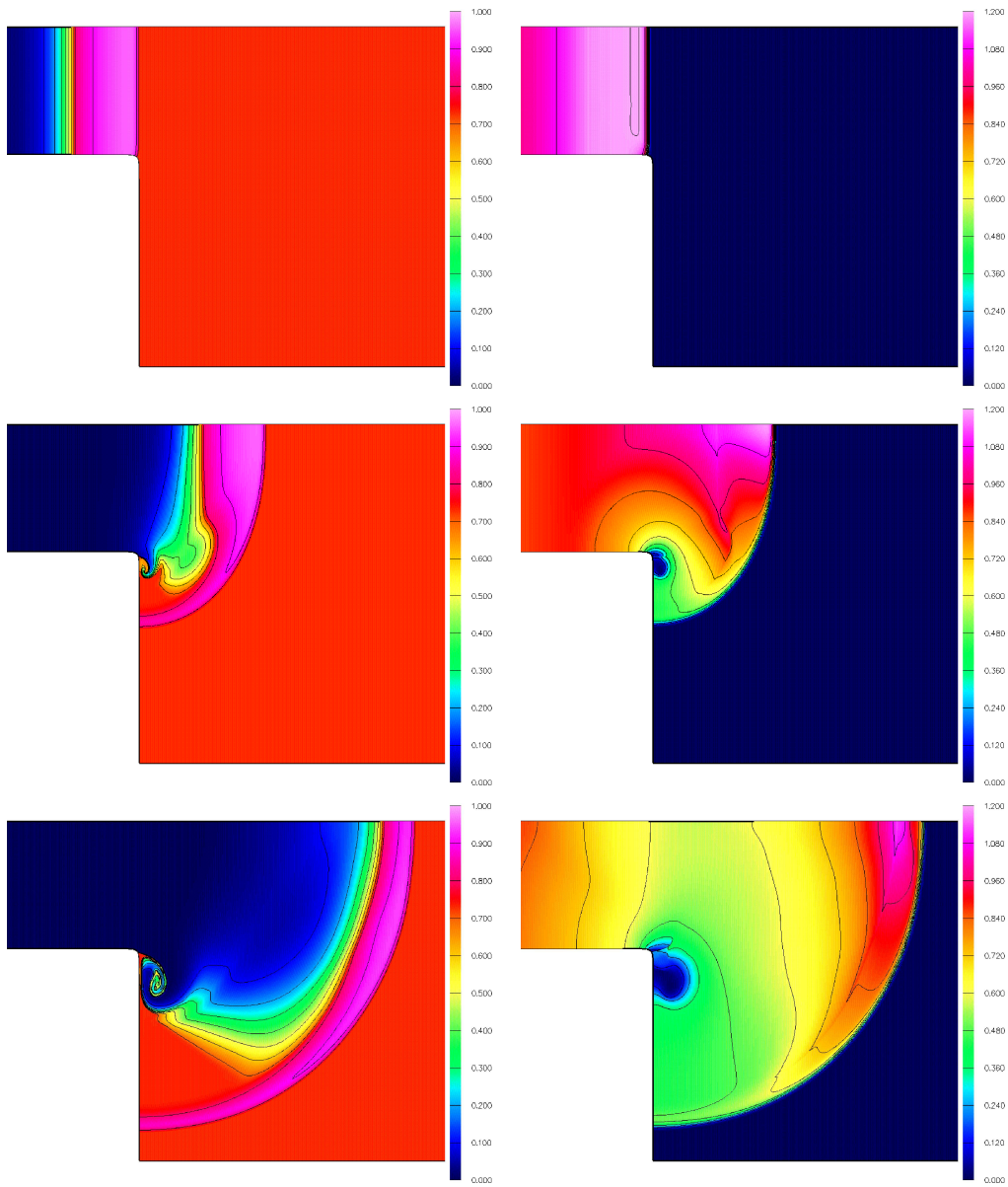

Figure 1: Shaded contours of the volume fraction of solid (left) and the gas pressure (right) for $t = 1.0$ (top), $t = 2.5$ (middle) and $t = 4.5$ (bottom).

Param.	Value	Param.	Value	Param.	Value
$\bar{\alpha}_0$	0.73	$\bar{\gamma}$	5	δ	20.
$\bar{\rho}_0$	5.0293	$\bar{\pi}$	0.16021	μ_c	0.05
$\bar{p}_0$	3.5682e−4	$\bar{C}_v$	0.625	$\mathcal{H}$	0.2
$\bar{T}_0$	1.2770e−2	q	0.11795	σ_{ign}	2.7
ρ_0	2.6470e−3	γ	1.35	σ_{burn}	6.0
p_0	1.1843e−5	b	0.37778	$p_{\min}$	0.5
T_0	1.2770e−2	C_v	1	$\phi_{\min}$	0.2

Table 1: Dimensionless parameters and their corresponding values for the corner-turning problem. The references scales are the same as those used in [6]. The values in the left two pairs of columns correspond to those for a representative PBX-type explosive, while the values in the right column are modeling choices.

algorithm. All elements of the AMR algorithm, such as error estimation, regridding, and interpolation, are performed in parallel. The approach developed may be used to compute the numerical solution of a wide range of initial-boundary-value problems (IBVPs) for partial differential equations. Details of the numerical approach are discussed in [12]. In that paper, IBVPs for two specific equations are discussed. The first is a linear advection-diffusion equation, and the second is the (nonlinear) reactive Euler equations. The first equation provides a useful test case to study the behavior of the numerical approach and to verify its accuracy quantitatively, while the second builds on the earlier work in [13, 14] and illustrates the numerical approach for a more difficult set of equations. For the purposes of this report, an overview of the numerical approach is given and some sample calculations from [12] are discussed.

3.2.1 Reactive Euler equations and numerical discretization

The numerical approach is illustrated for reactive and non-reactive flow in three-dimensions. Here, we assume inviscid compressible flow and consider the reactive Euler equations given by

$$\frac{\partial \mathbf{u}}{\partial t} + \frac{\partial}{\partial x_1}\mathbf{f}_1(\mathbf{u}) + \frac{\partial}{\partial x_2}\mathbf{f}_2(\mathbf{u}) + \frac{\partial}{\partial x_3}\mathbf{f}_3(\mathbf{u}) = \mathbf{h}(\mathbf{u}), \tag{2}$$

where

$$\mathbf{u} = \begin{bmatrix} \rho \\ \rho\mathbf{v} \\ E \\ \rho\mathbf{Y} \end{bmatrix}, \qquad \mathbf{f}_n = \begin{bmatrix} \rho v_n \\ \rho v_n \mathbf{v} + p\mathbf{e}_n \\ v_n(E+p) \\ \rho v_n \mathbf{Y} \end{bmatrix}, \quad n = 1,2,3, \qquad \mathbf{h} = \begin{bmatrix} 0 \\ \mathbf{0} \\ 0 \\ \rho\mathbf{R} \end{bmatrix}.$$

The symbols here have their usual meaning, namely, ρ is density, $\mathbf{v} = (v_1, v_2, v_3)$ is velocity, p is pressure and E is the total energy. For the reactive case, the flow is a mixture of m_r species whose mass fractions are given by $\mathbf{Y}$. The source term models the chemical reactions and is described by a set of m_r rates of species production given by $\mathbf{R} = \mathbf{R}(\mathbf{u})$. The total energy is taken to be

$$E = \frac{p}{\gamma - 1} + \frac{1}{2}\rho|\mathbf{v}|^2 + \rho q,$$

where γ is the ratio of specific heats and $q = q(\mathbf{Y})$ represents the heat energy due to chemical reaction. The number of components in the equations is $m = 5 + m_r$, but this reduces to $m = 5$ for the non-reactive case where we omit the m_r species equations in (2). The initial conditions for the equations are $\mathbf{u}(\mathbf{x}, 0) = \mathbf{u}_0(\mathbf{x})$ and the boundary conditions consist of inflow, outflow or solid-wall conditions as needed for each specific problem considered.

The discretization of the reactive Euler equations in (2) follows that discussed previously in the context of two-phase flow. For each component grid there is a known mapping $\mathbf{x} = \mathbf{C}_g(\mathbf{r})$ from physical space $\mathbf{x}$ to parameter space $\mathbf{r} \in [0,1]^3$. In parameter space, the equations become

$$\frac{\partial \mathbf{u}}{\partial t} + \frac{1}{J}\frac{\partial}{\partial r_1}\hat{\mathbf{f}}_1(\mathbf{u}) + \frac{1}{J}\frac{\partial}{\partial r_2}\hat{\mathbf{f}}_2(\mathbf{u}) + \frac{1}{J}\frac{\partial}{\partial r_3}\hat{\mathbf{f}}_3(\mathbf{u}) = \mathbf{h}(\mathbf{u}), \tag{3}$$

where J is the Jacobian of the transformation matrix $[\mathbf{x_r}]$ and the mapped fluxes $(\hat{\mathbf{f}}_1, \hat{\mathbf{f}}_2, \hat{\mathbf{f}}_3)$ are given in terms of the original flux functions by

$$\hat{\mathbf{f}}_\alpha(\mathbf{u}) = s_{\alpha,1}\mathbf{f}_1(\mathbf{u}) + s_{\alpha,2}\mathbf{f}_2(\mathbf{u}) + s_{\alpha,3}\mathbf{f}_3(\mathbf{u}), \qquad \alpha = 1,2,3.$$

Here, the metrics $s_{i,j}$ are components of the matrix $S = J[\mathbf{r_x}] = J[\mathbf{x_r}]^{-1}$, i.e.

$$s_{1,1} = \det\begin{bmatrix} \frac{\partial x_2}{\partial r_2} & \frac{\partial x_2}{\partial r_3} \\ \frac{\partial x_3}{\partial r_2} & \frac{\partial x_3}{\partial r_3} \end{bmatrix}, \quad s_{1,2} = \det\begin{bmatrix} \frac{\partial x_3}{\partial r_2} & \frac{\partial x_3}{\partial r_3} \\ \frac{\partial x_1}{\partial r_2} & \frac{\partial x_1}{\partial r_3} \end{bmatrix}, \quad s_{1,3} = \det\begin{bmatrix} \frac{\partial x_1}{\partial r_2} & \frac{\partial x_1}{\partial r_3} \\ \frac{\partial x_2}{\partial r_2} & \frac{\partial x_2}{\partial r_3} \end{bmatrix}, \quad \text{etc.}$$

The mapped flux $\hat{\mathbf{f}}_\alpha(\mathbf{u})$ represents the flux of $\mathbf{u}$ across the surface $r_\alpha =$ constant. Finally, the source term $\mathbf{h}(\mathbf{u})$ in the mapped equations is unchanged from the original set.

The mapped equations are discretized on a uniform grid with grid spacings Δr_α, $\alpha = 1,2,3$. Let

$$\mathbf{U_i}(t) = \frac{1}{\Delta r_1 \Delta r_2 \Delta r_3}\iiint_{V_\mathbf{i}} \mathbf{u}(\mathbf{r}, t)\, d\mathbf{r}$$

denote the average of $\mathbf{u}$ over a grid cell $V_\mathbf{i}$ of width $(\Delta r_1, \Delta r_2, \Delta r_3)$ about the point $\mathbf{r_i}$. The cell average of $\mathbf{u}$ is advanced from a time t to $t + \Delta t$ using the second-order fractional-step method

$$\mathbf{U_i}(t + \Delta t) = \mathcal{S}_h(\Delta t/2)\mathcal{S}_f(\Delta t)\mathcal{S}_h(\Delta t/2)\mathbf{U_i}(t),$$

where $\mathcal{S}_h$ and $\mathcal{S}_f$ are operators representing discretizations of the source term and the hydrodynamic terms of the mapped equations, respectively, and where Δt is a global time step determined for all component grids by a CFL condition. The integration of the source term is handled with a Runge-Kutta error-control scheme and the integration of the hydrodynamic terms are performed using a second-order extension of Godunov's method with an approximate Riemann solver.

3.2.2 Parallel framework

The parallel framework is a domain-decomposition approach in which each component grid belonging to the overlapping grid is partitioned across different processors of a distributed-memory parallel computer as illustrated in Figure 2. The sample overlapping grid in the

figure, shown in two dimensions for simplicity, consists of component grids labeled G_1 and G_2 at the base level, with G_2 cutting a hole in G_1, and refinement grids labeled G_3 and G_4. Each component grid is partitioned over a contiguous range of processors, e.g. $p = \{3, 4, 5\}$ for G_3. Grid functions defined on each component grid are partitioned in the same way as their component grid. Field data in a grid function, which may be distributed across several processors, is stored in a multidimensional P++ array. The P++ array, as described below, handles the updating of field data at ghost points associated with internal boundaries between processors. In addition, communication is needed between processors to update interpolation points at the overlap between grids (the grid points marked with small squares in Figure 2) and to handle AMR interpolation involving values on refinement grids.

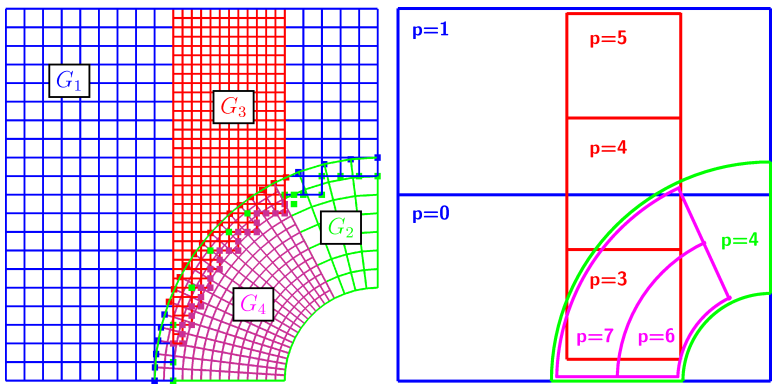

Figure 2: Sample overlapping grid showing a partition of base grids, G_1 and G_2, and a partition of refinement grids, G_3 and G_4, for parallel computation.

A basic tool for the parallel approach is the P++ array class [15], a C++ class that can be used to represent distributed multi-dimensional arrays. Each P++ array can be independently partitioned across a set of processors. A distributed P++ array consists of a set of serial arrays, one serial array for each processor. Each serial array is a multi-dimensional array that can be manipulated using various array operations. The data from a serial array can also be passed to Fortran subroutines, which is useful to define optimized computational kernels, such as the discretization of the reactive Euler equations representing an integration over a time step. When running in parallel, the serial arrays contain extra ghost values that hold copies of the data from the serial arrays on neighboring processors. The P++ array class is built on top of the Multiblock PARTI parallel communication library [16], which is used for updating the values on ghost boundaries from neighboring processors. All parallel communication is performed using the Message Passing Interface, MPI [17]. Further details of the parallel approach, including the parallel interpolation at grid overlaps, AMR regridding and interpolation, and method of load balancing are discussed in [12].

3.2.3 Sample results

Two problems involving three-dimensional reactive and non-reactive flow are presented in [12]. The first problem involves planar shock diffraction by a sphere, while the second considers the initiation and propagation of a detonation in a T-shaped pipe. As an example,

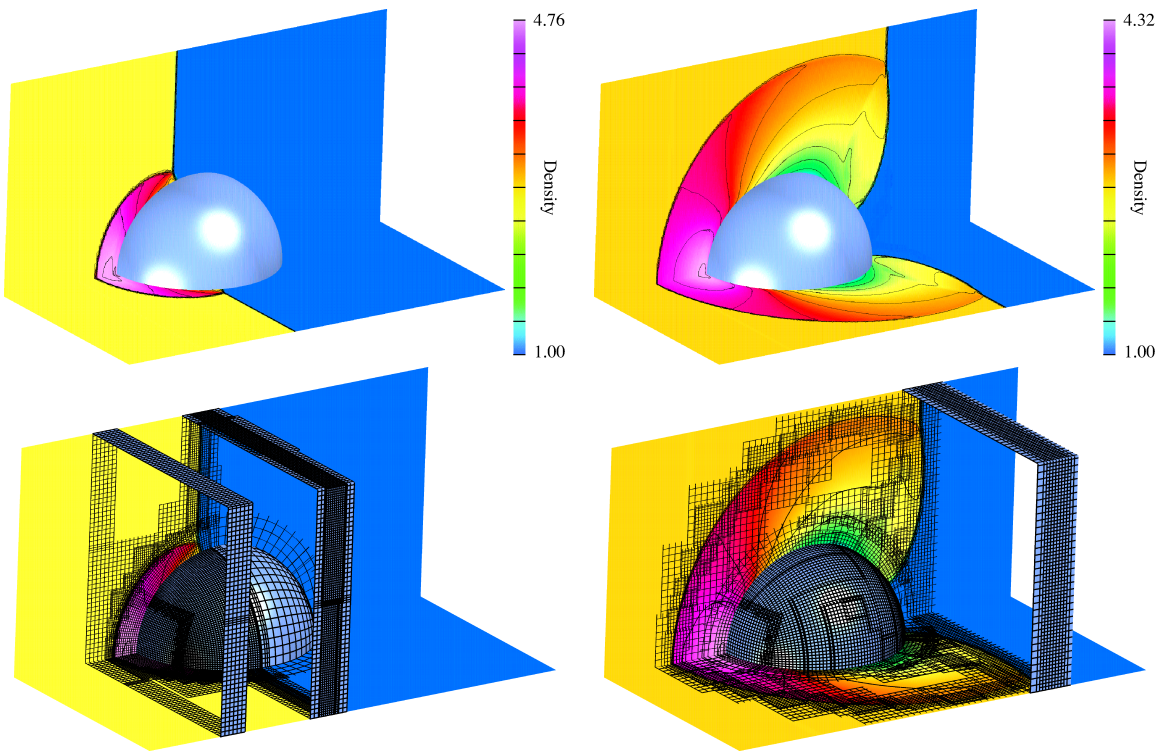

Figure 3: Shaded contours of density for the quarter-sphere problem at $t = 0.6$ (top left) and $t = 1.4$ (top right) with corresponding refinement-grid structure shown below each contour plot.

Figure 3 shows the density and the corresponding refinement grid structure of the solution of the shock-diffraction problem at two different times during the interaction of the shock with the solid sphere. This particular calculation was run using AMR with 2 refinement grid levels and using 32 processors. The parallel performance of the implementation was studied using a range of grids and number of processors. For example, Table 2 shows strong scaling results for calculations with no AMR. For each run, the overlapping grid is fixed, while the number of processors is increased from 1 to 64. The table lists the number of grids points, $\mathcal{N}^{(k)}_{\text{point}}$, number of processors, $N^{(k)}_{\text{proc}}$, points per processor, and the number of time steps taken, $\mathcal{N}^{(k)}_{\text{step}}$, for each run k. For each run, the CPU time per step, $\mathcal{T}_k$ (in seconds), is recorded and listed in the table, as well as the *parallel scale factor*, $\mathcal{S}_k$ which is computed using

$$\mathcal{S}_k = \frac{\mathcal{T}^*_0}{\mathcal{T}^*_k}, \qquad \text{where} \quad \mathcal{T}^*_k = \frac{\mathcal{T}_k}{\mathcal{N}^{(k)}_{\text{point}}/N^{(k)}_{\text{proc}}}.$$

Ideally, $\mathcal{S}_k = 1$, but since there is a cost associated with the communication between processors $\mathcal{S}_k < 1$. The table indicates good parallel scaling of the code for the shock diffraction problem. Further scaling results are given in [12].

k	$\mathcal{N}_{\text{point}}^{(k)}$	$N_{\text{proc}}^{(k)}$	$\mathcal{N}_{\text{point}}^{(k)}/N_{\text{proc}}^{(k)}$	$\mathcal{N}_{\text{step}}^{(k)}$	$\mathcal{T}_k$	$\mathcal{S}_k$
0	2.01e+6	1	2.01e+6	617	15.2	1.00
1	2.01e+6	2	1.00e+6	617	7.77	0.98
2	2.01e+6	4	5.02e+5	617	3.96	0.96
3	2.01e+6	8	2.51e+5	617	2.09	0.91
4	2.01e+6	16	1.26e+5	617	1.09	0.87
5	2.01e+6	32	6.27e+4	617	0.587	0.81
6	2.01e+6	64	3.14e+4	617	0.341	0.70

Table 2: Strong scaling results for the calculation of shock diffraction by a sphere with no AMR. The is the CPU time in seconds per step is given by $\mathcal{T}_k$. The parallel scaling factor $\mathcal{S}_k$ should be 1 for perfect parallel scaling.

4 Concluding Remarks

Work has continued on the development and use of adaptive numerical methods for the accurate calculation of various mathematical models of high-speed reactive and nonreactive flow. This work has focused on a two-phase reactive flow model. In addition, a parallel framework has been implemented to compute the solution of partial differential equations on overlapping grids with adaptive mesh refinement. The parallel framework has been used to compute solutions of the reactive and non-reactive Euler equations in three space dimensions [12], and solutions of the equations for two-phase reactive flow in two space dimensions (and other sets of partial differential equations).

References

[1] W. D. Henshaw, OverBlown: a fluid flow solver for overlapping grids, user's guide, Tech. Rep. UCRL-MA-134288, LLNL (1999).

[2] W. D. Henshaw, OverBlown: a fluid flow solver for overlapping grids, reference guide, Tech. Rep. UCRL-MA-134289, LLNL (1999).

[3] J. B. Bdzil, R. Menikoff, S. F. Son, A. K. Kapila, D. S. Stewart, Two-phase modeling of deflagration-to-detonation transition in granular materials: A critical examination of modeling issues, Phys. Fluids 11 (2) (1999) 378–402.

[4] J. M. Powers, Two-phase viscous modeling of compaction in granular explosives, Phys. Fluids 16 (8) (2004) 2975–2990.

[5] M. R. Baer, J. W. Nunziato, A two-phase mixture theory for the deflagration-to-detonation transition (DDT) in reactive granular materials, Int. J. Multiphase Flow 12 (1986) 861–889.

[6] D. W. Schwendeman, C. W. Wahle, A. K. Kapila, A study of detonation evolution and structure for a model of compressible two-phase reactive flow, Combust. Theory and Modeling 12 (2007) 159–204.

[7] D. W. Schwendeman, C. W. Wahle, A. K. Kapila, The Riemann problem and a high-resolution Godunov method for a model of compressible two-phase flow, J. Comput. Phys. 212 (2006) 490–526.

[8] W. D. Henshaw, D. W. Schwendeman, An adaptive numerical scheme for high-speed reactive flow on overlapping grids, J. Comput. Phys. 191 (2) (2003) 420–447.

[9] W. D. Henshaw, D. W. Schwendeman, Moving overlapping grids with adaptive mesh refinement for high-speed flow, J. Comput. Phys. 216 (2) (2006) 744–779.

[10] E. Ferm, C. Morris, J. Quintana, P. Pazuchanic, H. Stacy, J. Zumbro, G. Hogan, N. King, Proton radiography examination of unburned regions in PBX 9502 corner turning experiments, Tech. Rep. LA-UR-01-3555, Los Alamos National Laboratory (2001).

[11] A. K. Kapila, D. W. Schwendeman, J. B. Bdzil, W. D. Henshaw, A study of detonation diffraction in the ignition-and-growth model, Combust. Theory and Modeling 11 (2007) 781–822.

[12] W. D. Henshaw, D. W. Schwendeman, Parallel computation of three-dimensional flows using overlapping grids with adaptive mesh refinement, J. Comput. Phys. (submitted).

[13] W. D. Henshaw, D. W. Schwendeman, An adaptive numerical scheme for high-speed reactive flow on overlapping grids, J. Comput. Phys. 191 (2003) 420–447.

[14] W. D. Henshaw, D. W. Schwendeman, Moving overlapping grids with adaptive mesh refinement for high-speed reactive and non-reactive flow, J. Comput. Phys. 216 (2) (2006) 744–779.

[15] D. Quinlan, A++/P++ class libraries, Research Report LA-UR-95-3273, Los Alamos National Laboratory (1995).

[16] A. Sussman, G. Agrawal, J. Saltz, A manual for the Multiblock PARTI runtime primitives, revision 4.1, Technical Report CS-TR-3070.1, University of Maryland, Department of Computer Science (1993).

[17] W. Gropp, E. Lusk, R. Thakur, Using MPI-2: Advanced Features of the Message-Passing Interface, The MIT Press, Cambridge, MA, 1999.